A&A 390, 481–489 (2002)
DOI: 10.1051/0004-6361:20020757

Astronomy & Astrophysics

Near-infrared properties of Blue Compact Dwarf Galaxies: The link between solar and low metallicity⋆

L. Vanzi[1], L. K. Hunt[2], and T. X. Thuan[3]

[1] ESO, Alonso de Cordova, 3107 Santiago Chile
[2] IRA/CAISMI - CNR, Largo E. Fermi 5, 50125 Firenze, Italy
[3] Astronomy Department, University of Virginia, Charottesville, VA 22903, USA

Received 4 March 2002 / Accepted 22 May 2002

Abstract. We have obtained near-infrared images and spectra of three blue compact dwarf galaxies of intermediate sub-solar metallicity Tol 35, Tol 3 and UM 462. This work is part of a larger project aimed to study the star formation and the stellar populations of low metallicity galaxies in the near-infrared. In this frame work galaxies of intermediate metallicity represent an important step in understanding the most extreme cases filling the gap between solar and very low metallicity galaxies. We have observed HII region like spectra in all three galaxies; in all cases the star formation episodes are only a few Myr old. Consistently with a young age our spectra show no evidence for stellar absorption features typical of supergiants, nor of [FeII] emission typical of supernovae. The K-band gas fraction ranges from 20 to 40% showing that gas emission can significantly contaminate broadband near-infrared colors in young metal-poor starbursts. We have detected molecular hydrogen in emission in all three objects. All sources show bright knots superimposed on a lower surface brighness envelope. The knots are identified with Super Star Clusters; six of them are present in UM 462. In all galaxies we detect the presence of an old stellar population.

Key words. galaxies: dwarf – galaxies: starburst – galaxies: stellar content – galaxies: individual: Tol 35, Tol 3, UM 462

1. Introduction

Since the discovery of the first two Blue Compact Dwarf (BCD) Galaxies by Sargent & Searle (1970) and Searle & Sargent (1972), and their identification by Thuan & Martin (1981) as a class of low-luminosity metal-deficient objects, the importance of these galaxies has increased. BCD galaxies are characterized by strong episodes of star formation as evidenced by the blue optical colors and the presence of bright emission lines in the optical spectra. They span a range of metallicities that goes from about a third solar down to $Z_{\odot}/51$ for I Zw 18, indicating a non-uniform star formation history possibly undergoing episodic bursts (Thuan 1991). The importance of these galaxies is obvious since they are forming stars in an environment that must be similar to that expected in primeval galaxies (Izotov & Thuan 1999). For this reason they are unique laboratories to study star formation as it occurred in the Universe during its earliest phases.

Izotov & Thuan (1999) have proposed, based on an extensive study of a sample of BCD galaxies, to use the oxygen abundance as an age indicator; all galaxies with 12 + log(O/H) $\leq$ 7.6 would be younger than 40 Gyr. However single star photometry of one BCD galaxy showed that this limit is actually 1 Gyr (Izotov & Thuan 2002). Another approach to the problem of the age is the study of the stellar populations based on deep multi-wavelength photometry. NIR colors are effective indicators of the age of a stellar population once the metallicity is known. However Vanzi et al. (2000) point out how, though the NIR colors of normal, active and starburst galaxies are fairly well understood, their interpretation in BCDs is not easy and certainly not free from ambiguity. This is mainly due to two factors, 1) the broadband photometry of BCDs is strongly affected by nebular emission and no reliable conclusion on the stellar population can be driven without correcting the colors for this effect, 2) the interpretation of the colors is complicated by the difficultiy of incorporating the effect of metallicity into the evolutionary models in a satisfactory way. The case of SBS 0335-052 (the second lowest metallicity BCD with $Z_{\odot}/40$) is a good testbench since none of the currently available models is able to reproduce the colors of this galaxy even after taking into account the nebular contribution. To measure the nebular contribution spectroscopy is necessary. NIR spectra also offer the unique opportunity to probe the molecular hydrogen warm phase and to study a number of features not accesible at other wavelengths. Our main motivation for studying BCDs with $Z > Z_{\odot}/10$ is to link the

Send offprint requests to: L. Vanzi, e-mail: lvanzi@eso.org
⋆ Based on observations obtained at the ESO-NTT in La Silla.

Table 1. Observational characteristics of the sample galaxies.

	Tol 35	Tol 3	UM 462
RA (2000)	13:27:06	10:06:33	11:52:37
Dec (2000)	−27:57:24	−29:56:09	−02:28:10
v (km s^{-1})	2023	865	1055
D (Mpc) [a]	30.3	10.2	15.3
$Z/Z_\odot$	1/6	1/6	1/9
m(B)	14.5	13.5	14.5
other names	Tol 1324-276	Tol 1004-296	Mrk1307
	IC4249	NGC 3125	UGC 6850

[a] See text for details.

Table 2. Log of the observations.

object	grism	$t_{\rm int}$ (min)	PA	aperture(″)
Tol 35	blue	32	124	$1 \times 3/1 \times 3.5$
Tol 35	red	28	124	$1 \times 3/1 \times 3.5$
Tol 3	blue	30	113	$1 \times 1.5/1 \times 3$
Tol 3	red	24	113	$1 \times 1.5/1 \times 3$
UM 462	blue	30	23	1×2
UM 462	red	24	23	1×2

Table 3. NIR emission lines, fluxes measured in 10^{-15} erg/s/cm^2.

line	$\lambda_{\rm rest}$	Tol 35 A	Tol 3 A	Tol 3 B	UM 462
[SIII]+Pa 8	0.953	23.5±0.5	48.2±0.3	12.8±0.3	8.7±0.3
Paδ	1.005	3.1±0.2	6.6±0.2	5.8±0.3	1.2±0.3
HeI	1.082	15.5±0.3	36.1±0.3	2.5±0.3	10.5±0.5
Paγ	1.093	4.1±0.2	11.8±0.3	1.7±0.3	2.3±0.3
[OI]	1.128	-	0.5±0.2	-	-
Paβ	1.282	8.3±0.2	18.2±0.2	4.1±0.2	4.6±0.3
?	1.498	0.2±0.1	-	-	0.6±0.2
Br13	1.611	0.2±0.1	-	-	-
Br12	1.641	0.2±0.1	1.2±0.3	-	-
Br11	1.681	0.4±0.1	0.8±0.1	-	0.3±0.1
HeI	1.701	0.2±0.1	0.5±0.1	-	-
Br10	1.736	0.5±0.1	1.2±0.1	-	-
Br9		3.7±?	0.4±0.1	-	-
Brδ	1.944	1.3±0.1	2.8±0.1	0.7±0.3	1.1±0.1
H_2(1–0)S(3)	1.957	0.2±0.1	0.2±0.1	-	-
HeI	2.058	0.6±0.1	1.8±0.1	-	0.6±0.1
HeI	2.113	-	0.3±0.1	-	-
H_2	2.121	0.2±0.1	0.6±0.1	-	0.1±0.1
Brγ	2.165	1.6±0.1	4.1±0.1	0.6±0.2	1.1±0.1
H_2	2.248	-	0.2±0.1	-	-
H_2	2.407	-	0.4±0.2	-	-
H_2	2.413	-	0.4±0.2	-	-

well-studied extremely metal deficient BCDs, like I Zw 18 and SBS 0335-052, with the dwarf irregulars at the other end of the metallicity range, such as the LMC ($Z_\odot/3$). The fact that the properties of sub-solar and very low metallicity dwarf galaxies could be smoothly connected is suggested by the finding of Guseva et al. (2000) that the number of Wolf-Rayet stars in these galaxies is an increasing function of the metallicity in agreement with the predictions of the models. We are particularly interested in the photometric and spectroscopic properties of BCDs, their star-formation process, dust, gas and H_2 content as a function of the metallicity. It is our opinion that this approach can put important constraints on the star formation history of BCDs and on star formation models.

The present paper is organized as follows. In Sect. 2 we present our new observations. Sect. 3 is devoted to the discussion of the spectra and Sect. 4 to the images. In Sect. 5 we summarize the conclusions of our work.

2. Observations

We have selected Tol 35, Tol 3 and UM 462 as representative of star formation at intermediate sub-solar metallicity. Their abundances are $Z_\odot/6$ for Tol 35 and Tol 3 (Kobulnicky et al. 1999) and $Z_\odot/9$ for UM 462 (Izotov & Thuan 1998; Guseva et al. 2000). All three galaxies display the Wolf-Rayet features at 4686 Å (Vacca & Conti 1992; Schaerer et al. 1999; Guseva et al. 2000). This is indicative of a recent and short star formation episode as shown by the evolution of the number of WR over O stars predicted by single population evolutionary models (e.g. Leitherer & Heckman 1995). We have calculated distances to the sample galaxies using a Hubble constant H_0 of 70 km s^{-1} Mpc^{-1}, and the Virgo nonlinear flow model defined by Kraan-Korteweg (1986) and Giovanardi (2002). With this H_0 and the model of Kraan-Korteweg, the Virgo distance is 17.0 Mpc The characteristics of the galaxies are summarized in Table 1.

NIR spectra were observed with SOFI at the ESO NTT in 2000 April and 2001 April using the low resolution red and blue grisms which give a resolution $R = 600$ with a 1″ wide slit. The slit position angle (PA) was always chosen to include what seemed to be the most interesting regions in the Ks acquisition image. All galaxies were observed nodding along the slit. The Log of the observations is presented in Table 2. The reduction of the spectra was carried out in IRAF following the standard steps. 1D spectra centered on the brightest sources present in the slit were extracted with apertures that maximize the S/N, see Table 2. The telluric absorption features were removed from the spectra dividing by the spectrum of an O or G type star, then the original spectral shape was reestablished by multiplying by a black-body of suitable temperature in the first case or by the solar spectrum in the second one. The spectra were flux calibrated using the photometry of broadband images within the spectra extraction apertures. The agreement between the slope of the spectra and the photometry was at the 10% level for Tol 3 and Tol 35 and at the 20% level for UM 462. For this reason a correction factor was applied to the spectra. The comparison between the spectral fluxes and the photometry was always done by integrating the spectrum over the filters bandpass. Since the atmosphere significantly affects transmission, especially in the J filter its effect was included as well. The flux-calibrated spectra are displayed in Figs. 1, 2 and 3. The detected emission lines are listed in Table 3.

Broadband images in the J, H and Ks NIR filters were acquired with SOFI at the ESO-NTT in 2000 July. The integration time was 10 min per filter for all galaxies. All galaxies

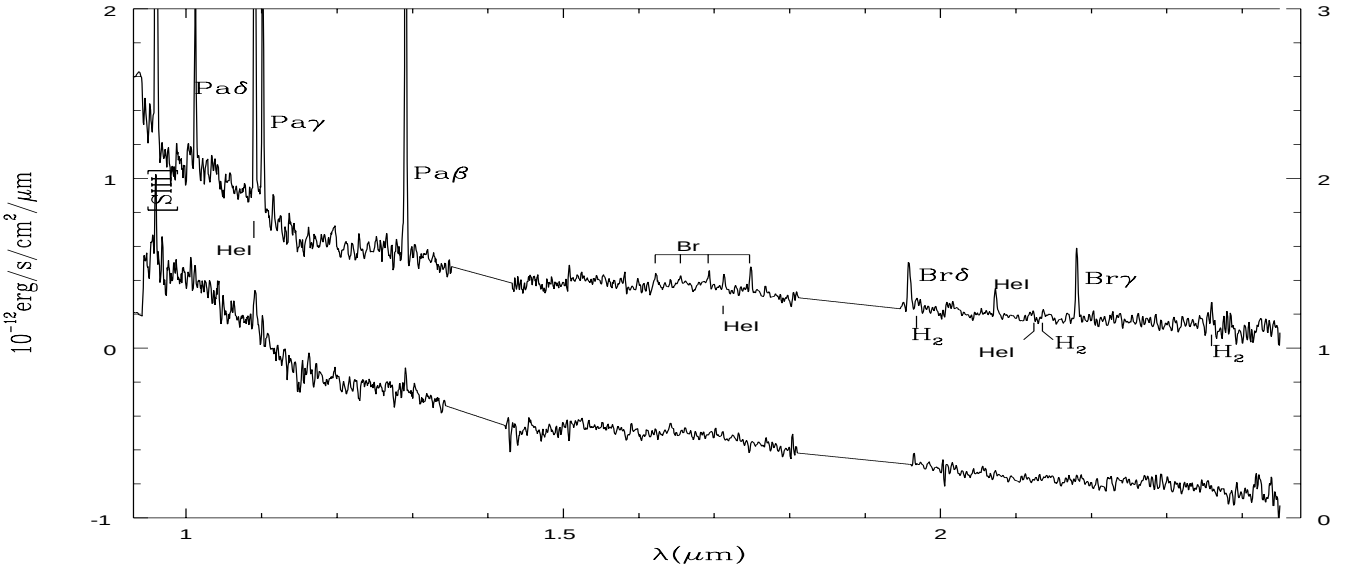

Fig. 1. NIR spectrum of Tol 35. The lower spectrum is extracted from the nucleus – region B (refear to flux in the right scale), the upper one from the brightest HII region in the galaxy – region A (refear to flux in the left scale). The regions of poor atmospheric transmission have been replaced by straight lines.

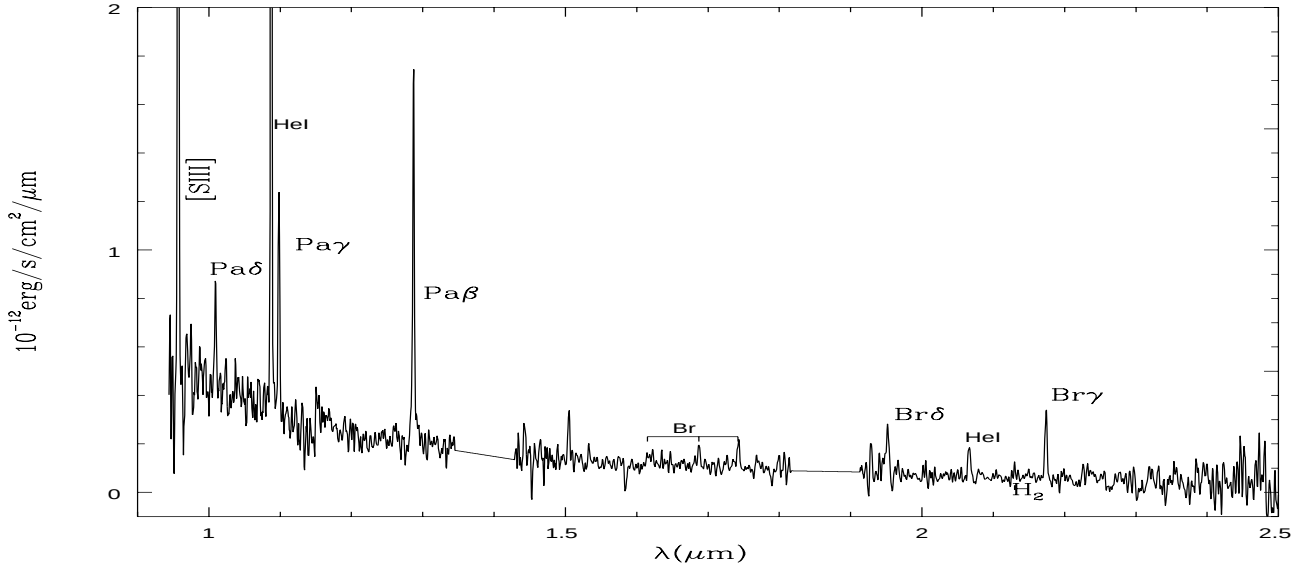

Fig. 2. NIR spectrum of UM 462 centered on region 1.

being small compared to the field of view they were observed dithering ON source. The images were reduced using the ESO Eclipse Package. The accuracy of the photometry was always better than 3%. Images of the three galaxies in the *K*s band are shown in Figs. 4, 5 and 6.

3. NIR spectra

In all three galaxies we have observed HII-region-like spectra with clear signatures of powerful episodes of star formation. These are the regions A in Tol 35 and Tol 3 (see Figs. 4 and 5) and region 1 in UM 462 (see Fig. 6). In particular, bright recombination lines of HI and HeI are detected in all the spectra.

3.1. Extinction and star formation rates

From the ratio of Paβ/Brγ it is possible to calculate the extinction toward the observed regions. We assume the intrinsic value 5.86 for the ratio as given by Hummer & Storey (1987) for $T = 10^4$ K and $n = 10^2$ cm^{-3} and the extinction law of Rieke & Lebofsky (1985). Galactic extinction is not negligible toward Tol 35 and Tol 3, $A_V = 0.270$ and 0.327 respectively, so that we have corrected for this effect first. Though the errors are large, a non-negligible extinction is observed in all cases. We obtain $A_V = 0.7 \pm 0.4$ in Tol 35 A, $A_V = 1.6 \pm 0.2$ in Tol 3 A, $A_V = 3.3 \pm 2.3$ in Tol 3 B and $A_V = 2.6 \pm 1.8$ in UM 462 1. These estimates are in good agreement with the optical values for the first two galaxies. Vacca & Conti (1992) give $A_V = 0.77$ for Tol 35 A and 1.97 for Tol 3 A. From the

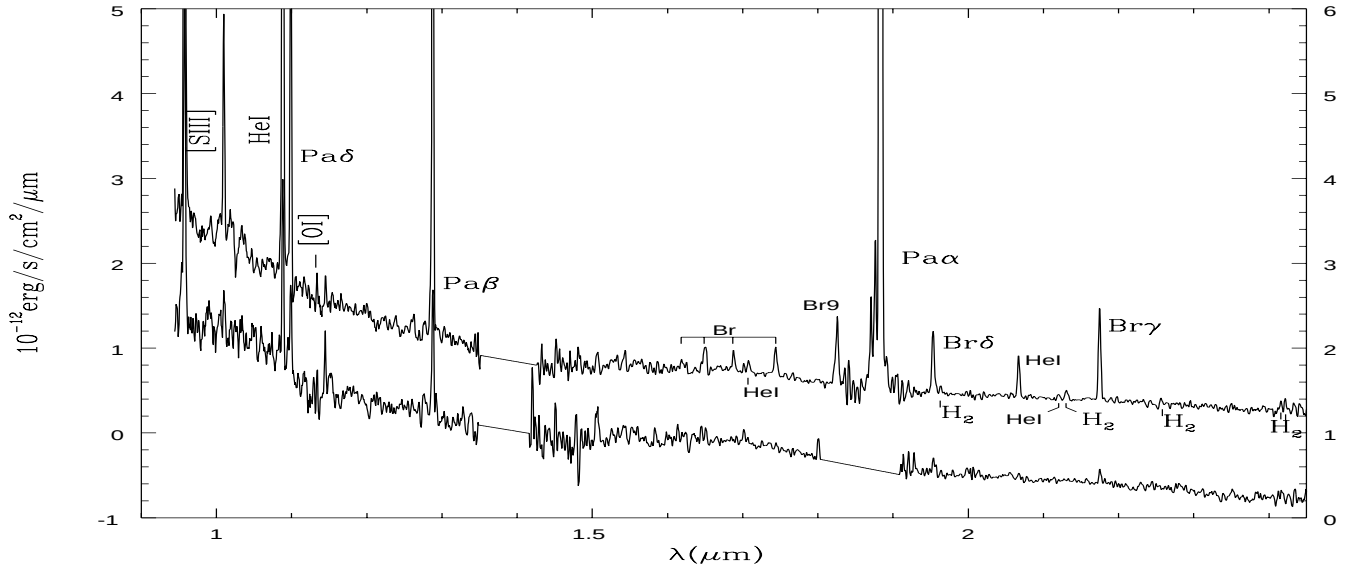

Fig. 3. NIR spectrum of Tol 3. The lower spectrum is extracted from region B (refear to flux in the right scale), the upper spectrum from region A (refear to flux in the left scale).

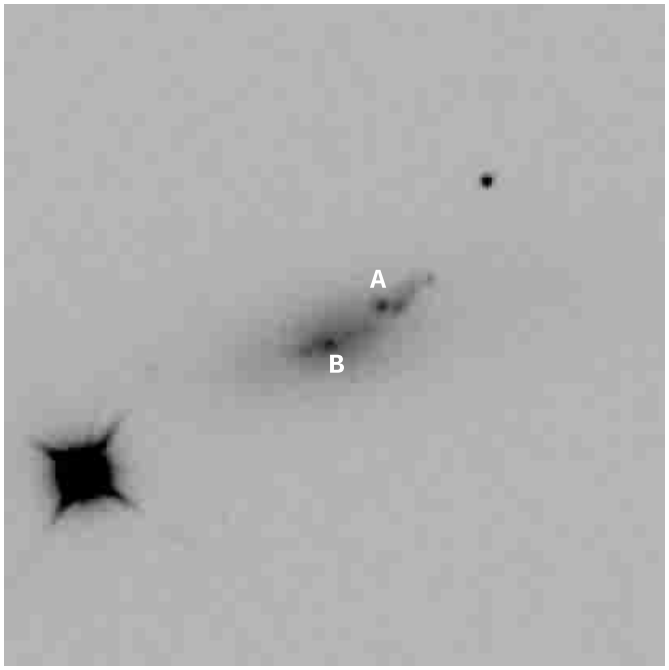

Fig. 4. Image of Tol 35 in *K*s. The field is 1×1 arcmin, north is up est at left. A and B mark the sources for which we extracted spectra.

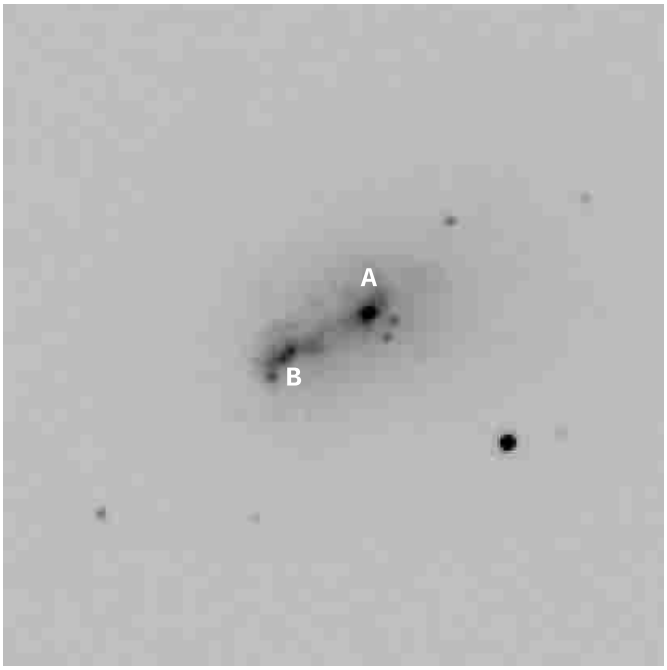

Fig. 5. Image of Tol 3 in *K*s. A and B mark the sources for which we extracted spectra. Field and orientation as in the previous images.

data of Terlevich et al. (1991) we derive $A_V = 0.26$ for UM 462 while Guseva et al. (2000) measure $A_V = 0.27$. Although the discrepancy in the case of UM 462 could be possibly due to a mis-match in slit position (the morphology of UM 462 seems in fact quite different in the optical and NIR – see Sect. 4), such a large difference could also be ascribed to the presence of hidden star formation somewhat similar to, but less extreme than in SBS 0335-052 (Hunt et al. 2001). Dust could be well present in UM 462 that has been detected by IRAS at 60 and 100 μm. We calculated the star formation rate in this galaxy using the global Hα flux from Guseva et al. (2000) (8.17×10^{-12} erg/s/cm^2) and the IRAS fluxes ($F_{60} = 0.944$ and $F_{100} = 0.896$ Jy) with the conversion factors of Kennicutt (1998) obtaining $SFR(\mathrm{H}\alpha) = 1.4\ M_\odot$/yr and $SFR(\mathrm{IR}) = 0.06\ M_\odot$/yr. From this comparison we do not find strong evidence to support the presence of hidden star formation so that the issue must be investigated further.

Based on our Brγ fluxes corrected for the extinction we measured a SFR of 0.28, 0.24 and 0.24 $M_\odot$/yr respectively in Tol 35 A, Tol 3 A and UM 462 or 4.4×10^{-3}, 3.3×10^{-2} and $2.2 \times 10^{-2}\ M_\odot$/yr/kpc^2.

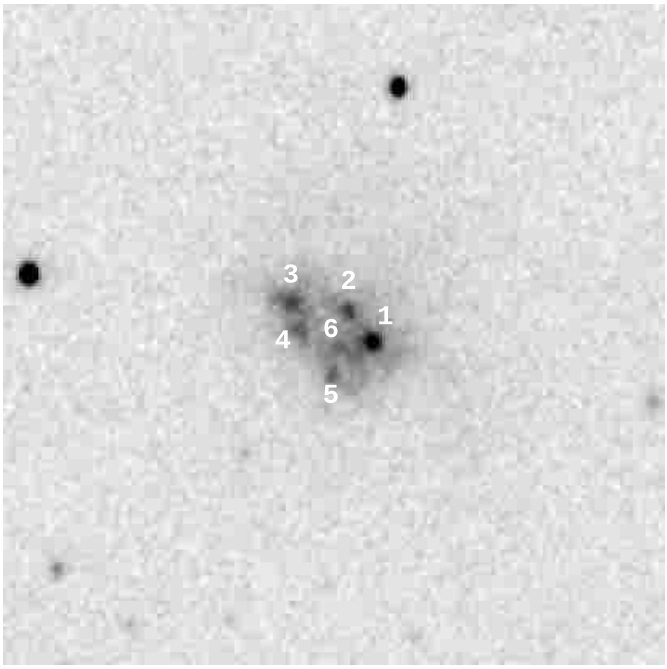

Fig. 6. Image of UM 462 in *K*s. Numbers from 1 to 6 mark the regions for which we extracted photometry. The spectrum is centered on region 1. Field and orientation as in the previous image.

3.2. Molecular hydrogen

Molecular hydrogen emission lines are detected in all galaxies. The (1,0)S(1)/Brγ ratios are 0.15, 0.12 and 0.09 respectively for Tol 3 A, Tol 35 A and UM 462. They are similar to the value measured in SBS 0335-520 by Vanzi et al. (2000) and perfectly consistent with the trend reported by Vanzi & Rieke (1997), suggesting that the H_2 emission is not affected, or it is affected at a low level, by the metallicity. The fact that the H_2 2.12 flux is only marginally affected by the metallicity in BCD galaxies is a remarkable finding: it tells us that H_2 is probably clumpy, confined to the star forming regions dust-enriched by SNe and not diffuse, consistently with the observations of FUSE (e.g. Vidal-Madjar et al. 2000; Thuan et al. 2002). The detection of the (1,0)S(3) transition in Tol 35 and Tol 3 is not significant enough to derive any conclusion on the excitation mechanism but the reddest part of the spectrum of Tol 3 is good enough to allow unambiguous detection of the transitions (2,1)S(1)2.248, (1,0)Q(1)2.407 and (1,0)Q(2)2.413. These detections strongly support the fluorescent excitation of H_2 as can be easily seen from the models reviewed by Engelbracht et al. (1998). Such a mechanism is quite natural in regions dominated by a strong UV field from young massive stars. From the similarity of the objects under study we can assume that the same mechanism is at work also in Tol 35 and UM 462 and explain the low (1,0)S(1)/Brγ ratio observed as produced by large "nude" clusters of young stars (Vanzi et al. 2000; Puxley et al. 1990).

3.3. [FeII] lines

The NIR lines of [FeII] are often used as indicators of supernovae in starburst galaxies (e.g. Vanzi & Rieke 1997) since the ratio [FeII]/Brγ has been found high (>20) in galactic SN remnants and low (<0.1) in galactic HII regions (Moorwood & Oliva 1988). [FeII] is not detected in any of the regions observed, either at 1.26 or at 1.64 μm, meaning that the spectra are dominated by young episodes of star formation where even the most massive stars have not yet had time to evolve to become SN. In other words the star formation observed in Tol 35 A, Tol 3 A and UM 462 must be younger than about 10 Myr. This conclusion is also supported by the very high equivalent width of Brγ, 90, 110 and 170 Å respectively in the 3 galaxies. According to Starburst99 (SB99, Leitherer et al. 1999), using an instantaneous burst, $Z_{\odot}/5$ and a Salpeter IMF, these correspond to ages between 5 and 7 Myr. Further support to the extreme youth of the observed episodes of star formation is given by the HeI lines. The HeI line at 1.700 μm is clearly detected in region A of Tol 3 and region A of Tol 35. The HeI line at 2.113 μm is detected in Tol 3 only. Both lines are strong signatures of the presence of young massive stars as discussed by Vanzi et al. (1996). The ratios HeI1.7/Br10 and HeI2.11/Brγ in Tol 3 A, respectively 0.42 and 0.07, and the ratio HeI1.7/Br10 = 0.40 in Tol 35 A, are in good agreement with the saturated values calculated by Vanzi et al. (1996). The two lines are not detected in UM 462 whose spectrum is however of lower quality. The presence of Wolf-Rayet stars in all three BCDs also gives an age of about 5–6 Myr for the young massive stellar population (Guseva et al. 2000).

3.4. Other spectral features

The [SIII] line at 0.953 μm is detected in all the spectra. Diaz et al. (1985) use this line as a diagnostic of the excitation mechanism. We took the ratio [SIII]/Paβ, after subtracting the contribution of Pa8 that is blended with [SIII] at our resolution, and converted it to [SIII]/Hα using a standard value for Hα/Pβ. Our values lie at the extreme high-excitation end of the HII region area in the plot of Diaz et al. (1985). This is easily explained by the low metallicity of our galaxies compared to the galactic HII regions used by other authors. The [SIII] line is in fact sensitive to the sulfur abundance (Rudy et al. 2001).

The CO absorption band at 2.29 μm can be used to constrain the age of the star-formation episode in starburst galaxies (Doyon et al. 1994), although it is not particularly reliable for ages older than roughly 10 Myr (Origlia & Oliva 2000), when red supergiants begin to emerge. In low metallicity environments, CO absorption is generally weak mostly because carbon abundance is lower, but also because stellar temperatures are warmer than those in more metallic systems (Origlia et al. 1997). Our NIR spectra reveal no absorption bands either at the CO(6,3) bandhead at 1.62 μm or at 2.29 μm, the CO(2,0) bandhead. In addition to the metallicity effect, this non-detection can be explained also by the young age of the bursts.

4. NIR images

4.1. Morphology and colors

As seen in the images presented in Figs. 4, 5, and 6, all galaxies show two or more bright knots of intense star-formation

Table 4. NIR magnitudes and colors observed on the spectroscopic apertures, gas fractions, corrections for the contribution of the ionized gas and colors of the extended regions of the galaxies.

Name		J	$J-H$	$H-K$	$(F_{\rm gas}/F_{\rm tot})_J$	$(F_{\rm gas}/F_{\rm tot})_H$	$(F_{\rm gas}/F_{\rm tot})_K$	$\Delta(J-H)$	$\Delta(H-K)$
Tol3	A	15.89	0.45	0.47	0.30	0.19	0.24	0.16	−0.08
	B	15.91	0.62	0.31	0.05	0.02	0.03	0.03	−0.01
	ext.		0.60	0.25					
Tol35	A	16.67	0.41	0.41	0.25	0.19	0.20	0.08	−0.01
	B	16.50	0.60	0.27	0.00	0.00	0.00	0.00	0.00
	ext.		0.55	0.18					
UM462		17.74	0.29	0.49	0.42	0.30	0.39	0.20	−0.15
	ext.		0.53	0.19					

activity, surrounded by low-surface brightness envelopes. Because of the non-ellipticity of its outer isophotes, UM 462 would be classified as iI according to the classification scheme of Loose & Thuan (1986). Tol 3 and Tol 35, on the other hand, present rather regular elliptical isophotes in the outer regions (although the foreground star disturbs the appearance toward the SE in Tol 35), and therefore would be classified as iE, the most common morphology of BCDs. In terms of morphology, Tol 3 and Tol 35 are reminiscent of I Zw 18, which is dominated by two main bright centers of star formation surrounded by a low surface-brightness envelope. UM 462 shows a peculiar morphology characterized by several knots of varying brightness, embedded within an irregular outer envelope. However a deeper B optical image of UM 462 by Cairós et al. (2001) does show that the outermost contours do become elliptical, and thus should be classified as iE. In all galaxies, the NIR colors and spectra of the knots differ, and may represent examples of propagating star formation (see Sect. 4.3).

To better constrain the colors of the extended regions, we have derived surface-brightness profiles of the galaxies. The profiles were extracted by first fitting elliptical isophotes to the J-band image, In Tol 3 and Tol 35, ellipse centers were fixed to the brightest knot (Tol 3A and Tol 35B); in the case of UM 462, the ellipse center was assigned to be the center of symmetry of the outer isophotes. In this case, the surface brightness peaks integrated azimuthally appear as a "shoulder" in the profile at $R \sim 3''$. While average-sigma clipping was performed for all objects, for Tol 35 it was also necessary to apply a mask in order to minimize the effect of the bright foreground star; nevertheless, the effects of the star appear in the profile at $R > 28''$. We note also that Tol 35B corresponds to the center of symmetry of the outer isophotes, and is most probably the nucleus of the galaxy. The surface-brightness profiles are described by exponential laws in Tol 35 and Tol 3 and by a higher order generalized exponential in UM 462. Mean colors of the outer regions of the galaxies were estimated from the profiles by averaging; these are shown by horizontal dashed lines in the lower panels of Figs. 8 and 10 and reported in Table 4. We have calculated the colors in the spectroscopic apertures, and performed photometry of the bright knots. All colors have been corrected for Galactic extinction (Schlegel et al. 1998). For the knots, we used a photometric aperture roughly equal to the seeing width ($1''$), appropriate for characterizing colors of point sources superimposed on a variable background. In Table 4 we list the colors observed in the spectroscopic apertures, and the corrections for nebular emission. The continuum correction was estimated by using the coefficients in Joy & Lester (1988) and our Brγ fluxes. The correction for emission lines was calculated by summing over the lines in our spectra. Total gas fractions are also reported in Table 4, and range from 20–40% in the brightest knots; J band fractions tend to be slightly larger than those in Ks because of the strong emission lines around 1 μm. Such large gas fractions and the corresponding color corrections clearly illustrate how ionized gas significantly affects broadband colors of young HII regions.

4.2. Models

In Fig. 7, we compare our results with models: Tol 3 is represented by circles, Tol 35 by squares, and UM 462 by X's (with number of knot when applicable). Filled symbols show photometry for the spectroscopic aperture, and open ones the mean colors of the outer regions. For the spectral apertures, photometry corrected for gas emission is shown (first lines, then continuum+lines). SB99 models are shown for three metallicities: 1/20 (blue, solid line), 1/5 (green, dotted line), and solar (red, dashed line) for a Salpeter IMF with upper cut-off at 100 $M_\odot$. For 1/5 $Z_\odot$, ages of 4, 10, and 25 Myr are marked with arrows. The characteristic shape of the curves is given by the fact that young ages are characterized by the reddest $H-K$ colors, because of the dominant gas (continuum only in SB99) emission such emission can dominate the K band (see Vanzi et al. 2000). Empirical NIR colors of late-type and dwarf galaxies (de Jong 1996) are shown as a cyan-colored grid. The X's numbered from 1 to 6 correspond to the knots detected in UM 462, and will be discussed below.

As in the majority of BCDs, the colors of the extended emission are in quite good agreement with evolved stellar populations of 1/5 $Z_\odot$ to $Z_\odot$ metallicity. It is clear that in each of our sample galaxies, at metallicities from $Z_\odot/9$ to $Z_\odot/6$, the extended envelope is populated by evolved (age > 5 Gyr) stars. Judging from $J-H$, Tol 3 is the most evolved galaxy; the knot B colors are very similar to those of the extended envelope, and both are relatively red in $J-H$ and blue in $H-K$.

To compare the colors of the knots with the models, it is necessary to correct the observations for gas line emission,

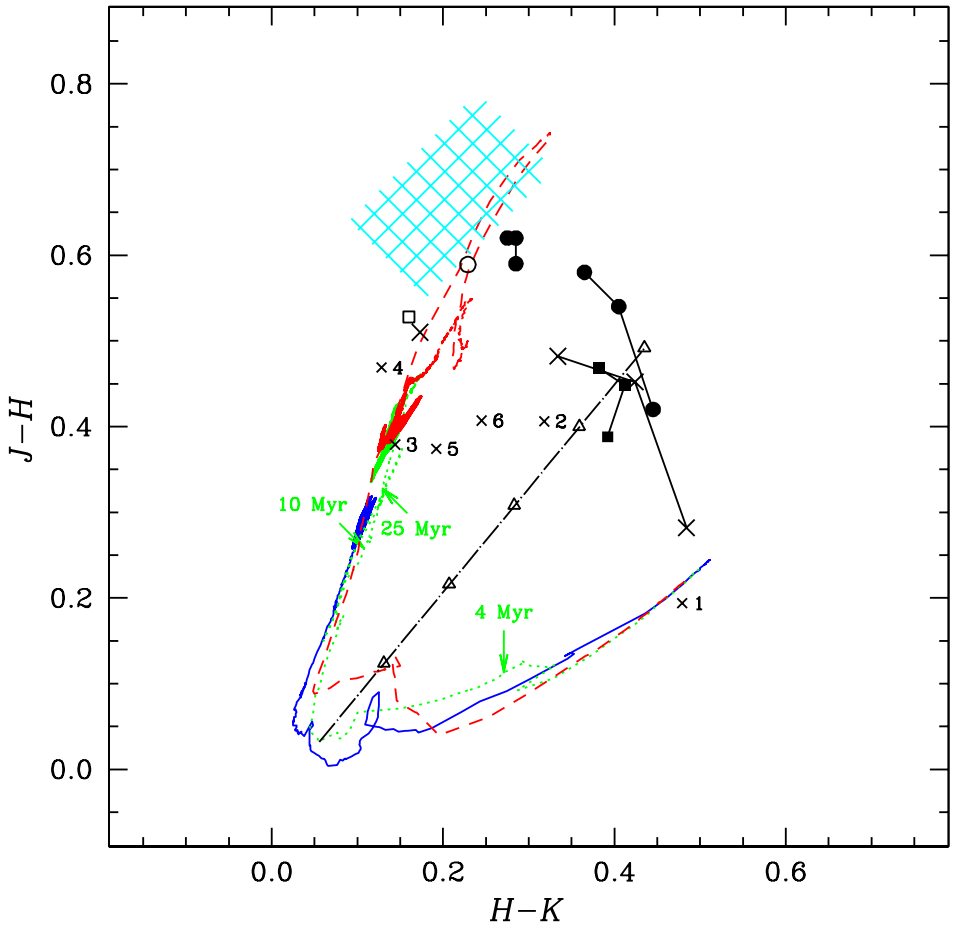

Fig. 7. $J-H$ vs. $H-K$ diagram for bright knots and extended regions of sample galaxies. Tol 3 is represented by circles, Tol 35 by squares, and UM 462 by crosses (with number of knot when applicable). Filled symbols show photometry for the spectroscopic aperture, and open ones the mean colors of the outer regions. Colors observed and corrected for the gas contribution are plotted and connected by solid lines. SB99 models are shown for three metallicities: 1/20 (blue, solid line), 1/5 (green, dotted line), and solar (red, dashed line). The cyan-colored grid rapresents the empirical NIR colors of late-type and dwarf galaxies. An extinction vector starts from the point of age 7 Myr on the $Z_{\odot}/5$ model, points corresponding to $A_V = 1$ are marked by open triangles.

since SB99 includes the contribution of the nebular continuum only. The only knot clearly compatible with the models is knot 1 in UM 462, although the colors have not been corrected for line emission. The remaining knots in Tol 3 (circles), Tol 35 (squares), and UM 462 (X's) are roughly compatible with a stellar population younger than 10 Myr, and a few magnitudes of extinction. Such young ages are consistent with the Brγ equivalent widths and the presence of HeI emission lines in our spectra; they are also consistent with the presence of Wolf-Rayet stars in these galaxies (Guseva et al. 2000; Vacca & Conti 1992).

The brightest knots in each galaxy show a peak red $H-K = 0.5$, in contrast to the surrounding $H-K$ color of 0.2. Such a red color is an almost certain signature of gas or hot dust, especially since we see no spectral sign of red supergiants but do detect large extinction and large gas fraction. The brightest knots also show a blue $J-H$ color: while the surrounding regions and the extended envelopes have $J-H = 0.5$–0.6, typical of evolved stellar populations, the bright knots have $J-H = 0.2$, consistent with young stars+gas (the $J-H$ color of gas including lines is ∼0.0–0.2). Such colors are indicative of extreme youth, since they are almost certainly due to a high gas fraction plus perhaps a small amount of hot dust that reddens $H-K$s.

While the data and the models appear to be in moderate disagreement, it should be borne in mind that the corrections for nebular emission and extinction are uncertain. Moreover, the corrected colors tend to be slightly redder than the models in $H-K$, which could point to the presence of hot dust (Vanzi et al. 2000). Indeed, 500 K dust does not affect $J-H$, but reddens $H-K$, making this color a strong diagnostic for hot dust emission.

4.3. Young Compact Star Clusters

Table 5 lists the photometric properties of the bright knots in the sample galaxies. All of the bright knots have absolute Ks magnitudes ranging from −12.5 in the weakest knot (#4 in UM 462) to −15.6 in Tol 35A; Tol 35B, the probable galactic nucleus, has $M_{K\mathrm{s}} = -15.8$, the brightest knot in our sample. These have not been corrected for gas emission, so are essentially upper limits; cluster #1 in UM 462 with a Ks gas fraction of ∼40%, would be diminished by roughly 0.6 mag.

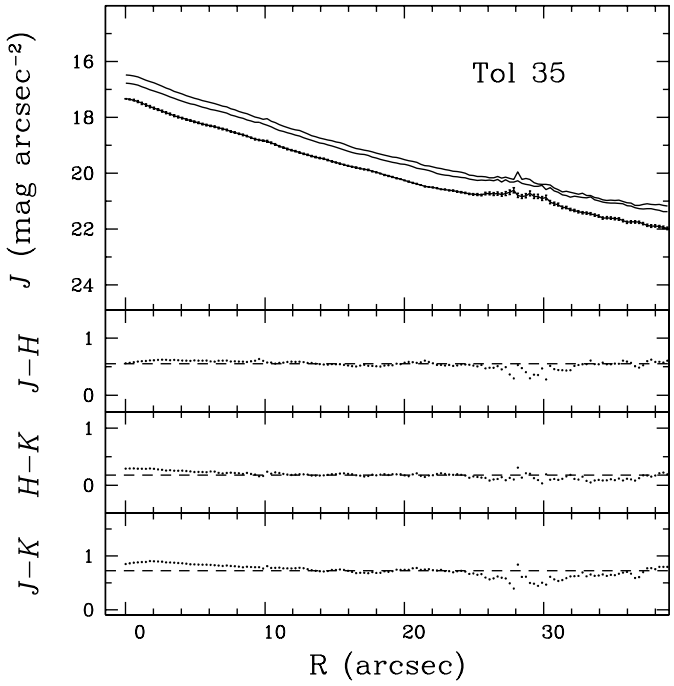

Fig. 8. Surface-brightness profiles of Tol 3 (left panel) and Tol 35 (right panel). In the upper panels, the J band profile is shown by data points with uncertainties, together with the H and Ks bands shown by solid lines. The lower panels show the radial variation of the NIR colors, with the mean colors of the outer isophotes shown as horizontal dashed lines. The surface-brightness profile of Tol 35 is compromised.

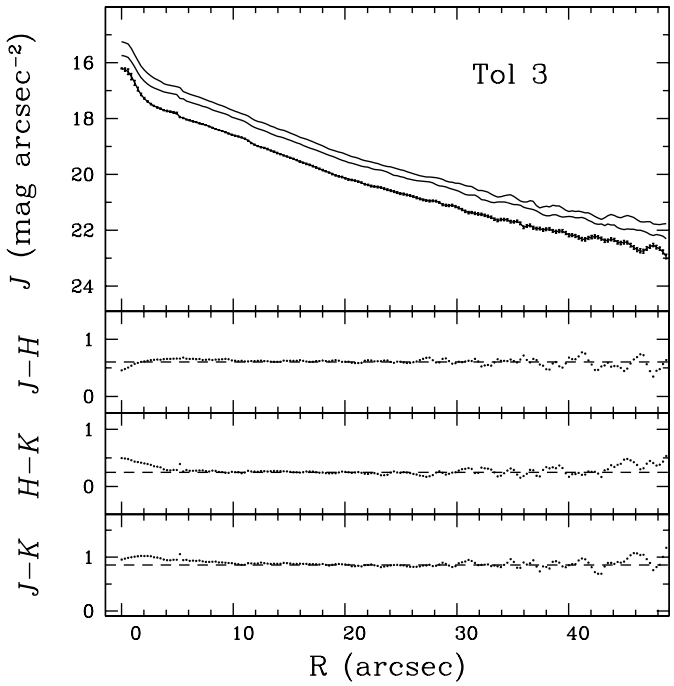

Fig. 9. Surface-brightness profiles of Tol 3. Same as previous figure.

We have measured the diameter of the clusters, taking into account the resolution limit dictated by our seeing (ranging from 0.8–1.1″ in Ks); 1″ corresponds to 50, 147, and 74 pc for Tol 3, Tol 35, and UM 462, respectively. Virtually all of the clusters are barely resolved or unresolved, having diameters

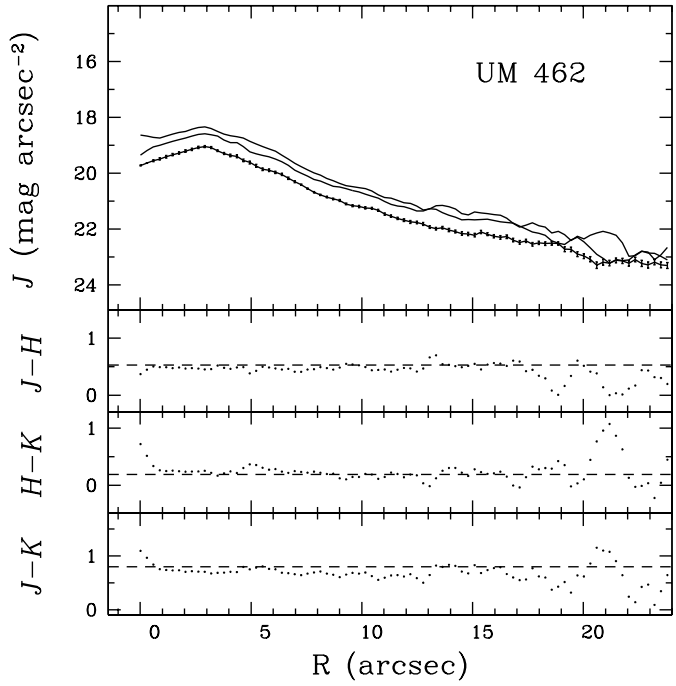

Fig. 10. Surface-brightness profiles of UM 462. Same as previous figure.

Table 5. SSC properties.

Name	Knot	$J-H$	$H-K$	Ks (1″)	M_{Ks}	Size (pc)
Tol3	A	0.47	0.46	15.32	−14.72	37
	B	0.64	0.29	16.13	−13.91	38
	B-tip	0.27	0.47	–	–	
Tol35	A	0.25	0.49	16.79	−15.61	72
	B	0.56	0.28	16.63	−15.78	173
UM462	1	0.19	0.48	17.61	−13.31	42
	2	0.41	0.32	18.14	−12.79	55
	3	0.38	0.14	18.20	−12.73	86
	4	0.47	0.13	18.38	−12.55	55
	5	0.37	0.19	18.45	−12.48	66
	6	0.41	0.25	18.45	−12.47	∼100

ranging from ∼40 pc in UM 462 and Tol 3 (the nearest galaxies) to ∼70 pc or larger in Tol 35 (the most distant). These are almost certainly size upper limits because of the seeing and distance constraints.

To derive the number of equivalent O7V stars in the regions observed spectroscopically and listed in Table 4, we first correct the Brγ fluxes for extinction, then multiply by 35.94 to convert to Hβ fluxes (for 100 cm^{-3} and T = 10 000 K, Osterbrock 1989). We then convert the Hβ fluxes to the number of Lyman continuum photons using the conversion factor given by Guseva et al. (2000). Adopting 10^{49} s^{-1} as the number of Lyman continuum photons for an O7V star, we obtain 462 O7V stars in Tol3 A, 1435 O7V stars in Tol 35 A, 695 O7V stars in Tol3 B, and 307 O7V stars in UM462-1. The absolute magnitudes, size and number of stars of the clusters

observed are indicative of Super Star Clusters (SSCs) (Billet et al. 2002; Whitmore 2000)

The SSCs in UM 462 vary in NIR color, and appear to follow a trend with age or gas fraction or both. Knot #1 has the reddest $H-K$s and bluest $J-H$ color, followed by the two nearest knots (#2 and #6). While $H-K$s gets bluer with increasing knot number (and distance from knot #1), $J-H$ remains roughly constant at 0.4 also for knots #3 and #5, but gets redder for knot #4. Such a trend suggests a decreasing gas fraction (because of the decreasing $H-K$s color) going from knot #1, #2, #6, to knot #4. This may also be interpreted as an age trend, since gas fraction decreases with age, and $J-H$ for knot #4 is slightly redder. Without spectral information for the different knots, it is difficult to be more definite. Nevertheless, the colors of the knots in UM 462 suggests that the star formation in knot is #1 is more recent than that in the remaining knots; knot #4 appears to be the oldest. The knots in Tol 3 show similar trends, with knot B appearing to be older than knot A. This is suggestive of propagating star formation, with the shock waves triggered by supernovae in the older knots triggering star formation in the younger knots.

5. Conclusions

The main results of this work are the following:

1. We have obtained NIR spectra and images of Tol 35, Tol 3 and UM 462 and detected bright HII regions in all them. The star-formation episodes are very young in the brightest regions, not older than few Myr.
2. Molecular hydrogen lines are present in all galaxies, and trends with metallicity suggest that in BCDs H_2 is clumpy, rather than diffuse.
3. Ks band gas fractions range from 3 to 40%, implying that ionized gas significantly affects broadband colors.
4. In all galaxies we detect the presence of Super Star Clusters. There are six of them in UM 462, arranged in an age or decreasing gas fraction sequence. The SSCs contain several hundred to more than 1000 O7V stars.
5. The low-surface brightness envelopes of all galaxies have NIR colors representative of evolved star.

Acknowledgements. We are grateful to Jason Spyromilio for generously sharing with us part of his observing time.

References

Billet, O. H., Hunter, D. A., & Elmegreen, B. G. 2002, AJ, 123, 1454
Cairos, L. M., Vilchez, J. M., Gonzalez Perez, J. N., Jglesias-Paramo, J., & Caon, N. 2001, ApJS, 133, 321
de Jong, R. S. 1996, A&A, 313, 377
Diaz, A. I., Pagel, B. E. J., & Wilson, R. G. 1985, MNRAS, 212, 737
Engelbracht, C. W., Rieke, M. J., Rieke, G. H., Kelly, D. M., & Achtermann, J. M. 1998, ApJ, 505, 639
Doyon, R., Joseph, R. D., & Wright, G. S. 1994, ApJ, 421, 101
Giovanardi, C. 2002, private comunication
Guseva, N. G., Izotov, Y. I., & Thuan, T. X. 2000, ApJ, 531, 776
Hummer, D. G., & Storey, P. J. 1987, MNRAS, 224, 801
Hunt, L. K., Vanzi, L., & Thuan, T. X. 2001, A&A, 377, 66
Hunt, L. K., Thuan, T. X., & Izotov, Y. I. 2002, submitted
Izotov, Y. I., & Thuan, T. X. 1998, ApJ, 500, 188
Izotov, Y. I., & Thuan, T. X. 1999, ApJ, 511, 639
Izotov, Y. I., & Thuan, T. X. 2002 [astro-ph/0111307]
Kennicutt, R. C. Jr. 1998, ARA&A, 36, 189
Kobulnicky, H. A., Kennicutt, R. C. Jr., & Pizagno, J. L. 1999, ApJ, 514, 544
Kraan-Korteweg, R. C. 1986, A&AS, 66, 255
Joy, M., & Lester, D. F. 1988, ApJ, 331, 145
Loose, H. H., & Thuan, T. X. 1986, in Star-forming Dwarf Galaxies and Related Objects, ed. Kunth, Thuan, & Tran Thanh van, 73
Leitherer, C., & Heckman, T. M. 1995, ApJS, 96, 9
Leitherer, C., Schaerer, D., Goldader, J. D., et al. 1999, ApJS, 123, 3
Melnick, J., & Mirabel, F. 1990, A&A, 231, L19
Moorwood, A. F. M., & Oliva, E. 1988, A&A, 203, 278
Origlia, L., Ferraro, F. R., Fusi Pecci, F., & Oliva, E. 1997, A&A, 321, 859
Origlia, L., & Oliva, E. 2000, A&A, 357, 61
Osterbrock, D. E., 1989, Astrophysics of gaseous nebulae and active galactic nuclei (Mill Valley University Science Books)
Puxley, P. M., Hawarden, T. G., & Mountain, C. M. 1990, ApJ, 364, 77
Rieke, G. H., & Lebofsky, M. J. 1985, ApJ, 288, 618
Rudy, R. J., Lynch, D. K., Mazuk, S., Puetter, R. C., & Dearborn, D. S. P. 2001 AJ, 121, 362
Schlegel, D. J., Finkbeiner, D. P., & Davis, M. 1998, ApJ, 500, 525
Sargent, W. L. W., & Searle 1970, ApJ, 162, L155
Schaerer, D., Contini, T., & Pindao, M. 1999, A&AS, 136, 35
Searle, L., & Sargent, W. L. W. 1972, ApJ, 173, 25
Terlevich, R., Melnick, J., Masegosa, J., Moles, M., & Copetti, M. V. F. 1991, A&AS, 91, 285
Thuan, T. X., & Martin, G. E. 1981, ApJ, 247, 823
Thuan, T. X. 1991, in Massive Stars in Starbursts, ed. C. Leitherer, N. R. Walborn, T. M. Heckman, & C. A. Norman (Cambridge Univ. Press), 183
Thuan, T. X., Levavelier des Etangs, A., & Izotov, Y. I. 2002, ApJ, 565, 941
Vacca, W. D., & Conti, P. S. 1992, ApJ, 401, 543
Vanzi, L., Rieke, G. H., Martin, C. L., & Shields, J. C. 1996, ApJ, 466, 150
Vanzi, L., & Rieke, G. H. 1997, ApJ, 479, 694
Vanzi, L., Hunt, L. K., Thuan, T. X., & Izotov, Y. I. 2000, A&A, 363, 493
Vidal-Madjar, A., Kunth, D., Lecavelier des Étangs, A., et al. 2000, ApJ, 538, L77
Whitmore, B. C. 2000 [astro-ph/0012546]